Computation of Multiple-Contact Frictional Equilibrium Postures in Three-Dimensional Gravitational Environments

Yizhar Or and Elon Rimon
Dept. of Mechanical Engineering, Technion, Israel
izi@tx.technion.ac.il, rimon@tx.technion.ac.il

Abstract *This paper is concerned with the problem of identifying equilibrium postures of a spatial mechanism supported by multiple frictional contacts in a three-dimensional gravitational field. The complex kinematic structure of the mechanism is lumped into a single rigid body, $\mathcal{B}$, with a variable center-of-mass and fixed contacts. The identification of the equilibrium postures associated with a given set of contacts is reduced to the identification of center-of-mass locations that maintain equilibrium of $\mathcal{B}$. The static response of $\mathcal{B}$ to an external wrench involves static indeterminacy and nonlinear frictional constraints. In this work we define a natural parametrization of the indeterminate contact forces for three-contacts postures, and derive an efficient approximation of the center-of-mass feasible region $\mathcal{R}$ in explicit closed form, accounting for the nonlinear friction constraints. Then we formulate the exact boundary of $\mathcal{R}$ as the solution of implicit high-order polynomials. For a general number of contacts, we show that computing $\mathcal{R}$ can be formulated as a projection of a high-dimensional region onto a two-dimensional plane. We then use polyhedral approximation of the quadratic friction cones, and apply an efficient algorithm for projection of high-dimensional convex polytopes to derive a polyhedral approximation of $\mathcal{R}$. Finally, we discuss the limitations of our work, and present some relevant open problems.*

1 Introduction

Quasistatic multi-legged locomotion on rough terrain in three dimensional environment requires criteria for identifying and computing equilibrium postures for the mechanism. This paper is concerned with the problem of identifying and computing the feasible equilibrium postures of a multi-limbed mechanism supported by a given set of frictional contacts in a three-dimensional gravitational field. In order to simplify the problem, we lump the complex kinematic structure of the mechanism into a single rigid body, $\mathcal{B}$, with a variable center of mass. The identification of the feasible equilibrium postures associated with a given set of contacts is reduced to the identification of center-of-mass locations that generate feasible equilibrium of $\mathcal{B}$, while satisfying the friction constraints at the contacts. A criterion for characterization of equilibrium postures in 3D can serve as a preliminary step towards 3D locomotion planning on rough terrain.

In the context of quasistatic locomotion under gravity in 2D, Bretl and Latombe [2] developed a motion planner for a three-legged planar robot climbing quasistatically on vertical walls with frictional supports. Erdmann et. al. [4] characterize the feasible center-of-mass positions for two frictional contacts in the context of nonprehensile palm manipulation. Or and Rimon [18] characterized multiple-contacts 2D equilibrium postures graphically and analytically and showed that the results are consistent with the planar graphical methods presented by Mason [12]. They also showed that computing center-of-mass feasible region can be formulated as a linear programming problem. In the three-dimensional case, however, Coulomb's model of friction, which has been experimentally verified [7],[13], is of quadratic nature. Therefore, the planar methods do not admit a straightforward generalization to the spatial case. In the context of multifingered frictional grasps in 3D, some works such as [20],[9],[10] used polyhedral approximation of the quadratic friction cones, which enables formulation of equilibrium tests and optimization problems as linear programs. Bicchi [1] formulated the force-closure test as a nonlinear differential equation. Trinkle et. al. [5] formulated the nonlinear frictional constraints as a linear matrix inequality (LMI) problem, for testing force-closure and optimizing actuator torques. The problem of computing feasible center-of-mass region for 3D frictional contact postures is more difficult, in the sense that it requires computation of a three-dimensional region (or its two-dimensional boundary) rather than optimization of a scalar cost function.

In the field of legged locomotion in 3D, the leading concept is the *support polygon principle* [16], which states that the center-of mass must lie above the polygon spanned by the contacts. This principle was further extended for dynamic motion synthesis of humanoid robots by using the concept of *zero moment point* (ZMP) [25],[24]. However, these concepts apply only for *flat surfaces*, where contact forces are vertical, and friction need not be considered. Mason et. al. [15] characterized 3D equilibrium postures on non-flat terrain with *frictionless* contacts. In order to synthesize legged motion on practical 3D environments, one needs to consider the terrain geometry as well as the nonlinear constraints imposed by friction. To our knowledge, this paper characterizes frictional equilibrium postures on 3D non-flat environments for the first time.

The structure of the paper is as follows. In the next section we formulate the equilibrium condition and frictional constraints, define the feasible center-of-mass region $\mathcal{R}$, and prove some of its fundamental properties. In section 3 we focus on three-contacts postures, and define a natural parametrization of the indeterminate contact forces. We use this parametrization to derive an efficient approximation of $\mathcal{R}$ in explicit closed form, accounting for the nonlinear friction constraints. We then formulate the exact boundary of $\mathcal{R}$ as the solution of implicit high-order polynomials. In section 4 we extend to a general number of contacts, and show that computing $\mathcal{R}$ can be formulated as a projection of a high-dimensional region onto a two-dimensional plane. We formulate the boundary of $\mathcal{R}$ as solution of systems of high-order polynomial equations. We then use polyhedral approximation of the quadratic friction cones, and apply an efficient algorithm for projection of high-dimensional convex polytopes to derive a polyhedral approximation of $\mathcal{R}$. In the closing section we conclude, discuss the limitations of our work, and present some relevant open problems.

2 Definition of Equilibrium Postures in 3D

We now define basic terminology and formulate the equilibrium conditions in 3D. Then we prove some basic properties of equilibrium postures in 3D. Let a solid object $\mathcal{B}$ be supported by k frictional contacts under gravity. Let x_i be the position of the i^{th} contact, and let $\vec{f_i}$ be the i^{th} contact reaction force. The static equilibrium condition is given by

$$\sum_{i=1}^{k} \begin{pmatrix} I \\ [x_i\times] \end{pmatrix} \vec{f_i} = - \begin{pmatrix} I \\ \boldsymbol{x}\times \end{pmatrix} \vec{f_g} \tag{1}$$

where $\boldsymbol{x}$ is the position of $\mathcal{B}$'s center-of-mass, f_g is the gravitational force acting at $\boldsymbol{x}$, I is the 3×3 identity matrix, and $[a\times]$ is the cross-matrix satisfying $[a\times]v = a \times v$ for all $v \in I\!R^3$. Note that for any $k \geq 3$ the static solution for $\vec{f_i}$ is generically indeterminate of degree $3k-6$. However, Assuming Coulomb's friction model, the contact forces $\vec{f_i}$ must lie in their respective friction cones

$$\mathcal{C}_i = \{\vec{f_i} : \vec{f_i} \cdot n_i \geq 0 \text{ and } (\vec{f_i} \cdot s_i)^2 + (\vec{f_i} \cdot t_i)^2 \leq (\mu \vec{f_i} \cdot n_i)^2\}, \tag{2}$$

where μ is the coefficient of friction, n_i is the outward unit normal at x_i, and s_i, t_i are unit tangents at x_i, such that (s_i, t_i, n_i) is a right-handed orthonormal frame. The friction constraints can also be written as the following linear and quadratic inequalities;

$$\mathcal{C}_i = \{\vec{f_i} : \vec{f_i} \cdot n_i \geq 0 \text{ and } \vec{f_i}^T B_i \vec{f_i} \leq 0\} \text{ , where } B_i = [s_i \;\; t_i \;\; n_i] \cdot \mathsf{diag}(1, 1, -\mu^2) \cdot [s_i \;\; t_i \;\; n_i]^T. \tag{3}$$

In this work, we assume that all contacts are *upward pointing*, in the sense that all forces $\vec{f_i}$ in $\mathcal{C}_i$ satisfy $\vec{f_i} \cdot e \geq 0$ where $\boldsymbol{e} = (0\ 0\ 1)$ denotes the upward vertical direction. This is a reasonable assumption in the context of legged locomotion, since relevant supports are generally located *under* the robot's footpads. We also assume that the coefficient of friction μ at all contacts is known. A 3D posture is defined by the contact points x_i and the center-of-mass position $\boldsymbol{x}$. For a given set of contacts $x_1 \ldots x_k$, the 3D feasible equilibrium region ,denoted $\mathcal{R}$, is all center-of-mass locations for which there exist contact reaction forces $\vec{f_i} \in \mathcal{C}_i$ that satisfy the static equilibrium condition (1). The goal of this paper is to compute the feasible region $\mathcal{R}$ for any given set of contacts. First, we present three fundamental properties of $\mathcal{R}$, summarized in the following lemma.

Lemma 2.1. *Given a solid body $\mathcal{B}$ supported by k frictional contacts under gravity, the feasible equilibrium region $\mathcal{R}$, if nonempty, is an infinite vertical prism. This prism is a single connected set and its cross-section is convex. Furthermore, if $\mathcal{R}$ is non-empty,its diension for k contacts is generically* $\min\{3, k\}$.

Proof: Let $\boldsymbol{e} = (0\ 0\ 1)$ denote the vertical direction. If $\boldsymbol{x} \in \mathcal{R}$, then the infinite vertical line $\{\boldsymbol{x} + \beta\boldsymbol{e}, \beta \in I\!R\}$ is contained in $\mathcal{R}$, since $\vec{f_g} \parallel \boldsymbol{e}$, and hence the right side of (1) is independent of β. Therefore $\mathcal{R}$ is an infinite vertical prism.
Next, let $\boldsymbol{x}'$ and $\boldsymbol{x}''$ be two points in $\mathcal{R}$, and let $\vec{f_i'}, \vec{f_i''} \in \mathcal{C}_i$ be the corresponding contact forces for $i = 1 \ldots k$. Let $\boldsymbol{x}(\lambda) = \lambda\boldsymbol{x}' + (1-\lambda)\boldsymbol{x}''$ for $\lambda \in [0, 1]$. It is easy to see that the contact forces $\vec{f_i} = \lambda\vec{f_i'} + (1-\lambda)\vec{f_i''}$ lie in $\mathcal{C}_i$ and satisfy (1) with $\boldsymbol{x} = \boldsymbol{x}(\lambda)$. Therefore $\mathcal{R}$ is connected as well as convex.

Finally, let us examine the dimension of $\mathcal{R}$. Consider the geometric implications of (1) in wrench space. On the right side of (1), $\boldsymbol{x}$ parametrizes a two-dimensional affine subspace L in wrench space. (Note that the component of $\boldsymbol{x}$ along $\boldsymbol{e}$ is mapped to zero). On the left side of (1), the contact forces $\vec{f}_i \in \mathcal{C}_i$ parametrize a cone N in wrench space. The intersection $N \cap L$ determines the horizontal components of all points $\boldsymbol{x}$ in $\mathcal{R}$, which gives the horizontal cross-section of $\mathcal{R}$. For a single contact, the cone N is 3-dimensional in wrench space. However, wrenches $(\vec{f}, \vec{\tau}) \in I\!R^6$ generated by a *single* force must satisfy the additional scalar constraint $\vec{f} \cdot \vec{\tau} = 0$. Therefore, if $N \cap L$ is nonempty, it is zero-dimensional[1], i.e. a single point in wrench space. Physically, $\mathcal{R}$ is the infinite vertical line passing through the single contact. When $k = 2$ the wrench cone N is *five*-dimensional, since $\vec{f}_1$ and $\vec{f}_2$ cannot generate torques about the line connecting x_1 and x_2. Therefore $N \cap L$ is generically one-dimensional. In this case $\mathcal{R}$ is an infinite vertical strip lying in the vertical plane passing through x_1 and x_2. When $k \geq 3$, N is a six-dimensional cone in wrench space, and $N \cap L$ is generically a two-dimensional region in wrench space. Each point in $N \cap L$ determines an infinite vertical line in $\mathcal{R}$, which is consequently three-dimensional. □

The analysis of the dimension of $\mathcal{R}$ was first presented in [15] for frictionless contact postures in 3D, and was extended here for the frictional case.

The problem of computing the prism $\mathcal{R}$ is thus reduced to computing its horizontal cross-section, denoted $\widetilde{\mathcal{R}}$, in $I\!R^2$. Since $k = 3$ is the smallest number of contacts for which $\mathcal{R}$ is fully three-dimensional, the next section focuses on the computation of $\widetilde{\mathcal{R}}$ for 3-contact postures.

The Support Polygon Principle: The classical *support polygon principle* appears in the legged locomotion literature [16], as a measure for frictionless postures' static stability on flat horizontal surfaces. This principle (also known as *the tripod rule* in 3-legged cases [15]) states that the center-of-mass must lie in a vertical prism whose horizontal cross section is the *support polygon* — the convex hull of the horizontal projections of all contact points. This principle is true also for the frictional case, as long as the supports are *nearly flat*, i.e. the upward direction $\boldsymbol{e}$ is contained in *all* friction cones $\mathcal{C}_i$. However, in the case of general non-flat supports where some of the friction cones *do not* contain $\boldsymbol{e}$, this principle cannot be applied. The method presented in this paper applies for contacts of any given geometry of non-flat supports, as long as all contacts are *upward pointing*.

[1] In general, if M is an m-dimensional manifold and N is an n-dimensional manifold in $I\!R^p$, the intersection $M \cap N$, if nonempty, has dimension $m + n - p$.

3 Postures Computation by Parametrization Approach

In this section we focus on 3-contact postures, and present a convenient parametrization of the static contact forces. We show that this parametrization leads to a natural description of the feasible region $\mathcal{R}$. Then we provide an approximation for the cross-section $\widetilde{\mathcal{R}}$ by formulating a partial set of its candidate boundary curves in explicit closed form. Next, we express the exact boundary curves as a solution of an implicit high-degree polynomial. We illustrate the approximate boundary and numerical solutions of the exact boundary by graphical examples.

3.1 Parametrizing Static Forces in 3-Contact Postures

We now focus on 3-contact postures and present a parametrization for the static reaction forces satisfying the equilibrium condition (1) and the frictional constraints (3). The resulting parametrization would be in terms of a parameter $\boldsymbol{r}$ which varies within a polygonal region in $I\!R^2$, and $\boldsymbol{\zeta}$ which varies in $I\!R^3$. First, let us decompose each contact force into its horizontal and vertical projections,

$$\tilde{f}_i = E^T \vec{f}_i \ \ , \ \ f_i^z = \boldsymbol{e} \cdot \vec{f}_i \ , \text{ where } E = \begin{pmatrix} 1 & 0 \\ 0 & 1 \\ 0 & 0 \end{pmatrix}.$$

Let $\tilde{\boldsymbol{x}} = E^T \boldsymbol{x}$ be the horizontal projection of $\boldsymbol{x}$. Then the equilibrium condition can be divided into three equation sets [15]

$$\begin{aligned} &a. \quad \textstyle\sum_{i=1}^3 \tilde{f}_i = 0_{2\times 1} \\ &\qquad \boldsymbol{e}^T \textstyle\sum_{i=1}^3 [x_i\times]\, E\tilde{f}_i = 0 \\ &b. \quad \textstyle\sum_{i=1}^3 f_i^z = 1 \\ &c. \quad \textstyle\sum_{i=1}^3 H_i\tilde{f}_i + h_i f_i^z = J^T\tilde{\boldsymbol{x}}, \end{aligned} \tag{4}$$

where $H_i = E^T[x_i\times]E$, $h_i = E^T[x_i\times]\boldsymbol{e}$, and $J = \left[\begin{smallmatrix} 0 & -1 \\ 1 & 0 \end{smallmatrix}\right]$. Note that the force units are scaled such that $\|\vec{f}_g\| = 1$. We will use (4a) and (4b) to obtain a parametrization of the contact forces, which will then imply a parametrization for $\boldsymbol{x}$ via Eq. (4c). The three scalar equations (4a) are force and torque balance of the three contact forces in a horizontal plane. These equations are independent of $\boldsymbol{x}$, contain six scalar unknowns, and hence are indeterminate of degree 3. Let $\tilde{x}_i = E^T x_i$ be the horizontal projection of the contact point x_i, and let $\tilde{\mathcal{C}}_i$ be the horizontal projection of the friction cone $\mathcal{C}_i$. In order to satisfy the friction constraints, $\tilde{f}_i$ must lie in $\tilde{\mathcal{C}}_i$. Since the horizontal forces $\tilde{f}_i$ generate zero net force and torque in the plane, they must intersect at a common point $\boldsymbol{r}$ in the plane. Since (4a) is homogenous in $\tilde{f}_i$, any particular choice of $\boldsymbol{r}$ determines $\tilde{f}_i$ up to a scaling factor $\sigma \in I\!R$. Therefore the pair $(\boldsymbol{r}, \sigma)$ fully parametrize $\tilde{f}_i$. Moreover, the frictional constraints imply that $\boldsymbol{r}$ must lie within a polygonal region in $I\!R^2$. These results are summarized in the following lemma.

Lemma 3.1. *Let $\boldsymbol{r}$ be a point in $\mathbb{R}^2$, and let $\sigma \in \mathbb{R}$ be a scaling factor. Then the horizontal contact forces solving Eq. (4a) are parametrized by $(\boldsymbol{r}, \sigma)$ as follows:*

$$\tilde{f}_i = \sigma\lambda_i(\boldsymbol{r})(\boldsymbol{r} - \tilde{x}_i) \ , \text{ where } \lambda_i(\boldsymbol{r}) = (\boldsymbol{r} - \tilde{x}_{i+1}) \cdot J(\tilde{x}_{i+2} - \tilde{x}_{i+1}) \ \ i = 1, 2, 3, \tag{5}$$

where the index i is taken modulo 3.
Furthermore, for any nontrivial solution satisfying $\tilde{f}_i \in \tilde{\mathcal{C}}_i$, $\boldsymbol{r}$ must lie within a union of two polygons $P = P_+ \cup P_-$, defined by:

$$\begin{aligned} P_+ &= \{\boldsymbol{r} : \ \ \mathsf{sgn}[\lambda_i(\boldsymbol{r})] \cdot (\boldsymbol{r} - \tilde{x}_i) \in \tilde{\mathcal{C}}_i \ , \ \boldsymbol{r} \neq \tilde{x}_i \ , \text{ for } i = 1, 2, 3\}, \\ P_- &= \{\boldsymbol{r} : \ \ -\mathsf{sgn}[\lambda_i(\boldsymbol{r})] \cdot (\boldsymbol{r} - \tilde{x}_i) \in \tilde{\mathcal{C}}_i \ , \ \boldsymbol{r} \neq \tilde{x}_i \ , \text{ for } i = 1, 2, 3\}. \end{aligned} \tag{6}$$

Proof: Eq. (4a) describes an equilibrium of three planar forces $\tilde{f}_1, \tilde{f}_2, \tilde{f}_3$. Since the three forces generate zero net torque, their lines must intersect at $\boldsymbol{r}$. Hence each force $\tilde{f}_i$ is directed from $\tilde{x}_i$ to $\boldsymbol{r}$ and can be written as $\tilde{f}_i = \sigma_i(\boldsymbol{r} - \tilde{x}_i)$ for some $\sigma_i \in \mathbb{R}$. The force part of (4a) can now be written as

$$\sigma_1(\boldsymbol{r} - \tilde{x}_1) + \sigma_2(\boldsymbol{r} - \tilde{x}_2) + \sigma_3(\boldsymbol{r} - \tilde{x}_3) = 0_{2\times 1}.$$

Taking dot product with $J(\boldsymbol{r} - \tilde{x}_1)$ and $J(\boldsymbol{r} - \tilde{x}_2)$, gives

$$\begin{aligned} (\boldsymbol{r} - \tilde{x}_2) \cdot J(\boldsymbol{r} - \tilde{x}_1)\sigma_2 + (\boldsymbol{r} - \tilde{x}_3) \cdot J(\boldsymbol{r} - \tilde{x}_1)\sigma_3 = 0 \\ (\boldsymbol{r} - \tilde{x}_1) \cdot J(\boldsymbol{r} - \tilde{x}_2)\sigma_1 + (\boldsymbol{r} - \tilde{x}_3) \cdot J(\boldsymbol{r} - \tilde{x}_2)\sigma_3 = 0 \end{aligned}$$

This is a homogenous linear system in $\sigma_1, \sigma_2, \sigma_3$. Its solution up to a scaling factor $\sigma \in \mathbb{R}$ is

$$\sigma_i = \sigma(\boldsymbol{r} - \tilde{x}_{i+2}) \cdot J(\boldsymbol{r} - \tilde{x}_{i+1}), \text{ where the index } i \text{ is taken modulo 3.}$$

Substituting the identity $(\boldsymbol{r} - \tilde{x}_{i+2}) \cdot J(\boldsymbol{r} - \tilde{x}_{i+1}) = (\boldsymbol{r} - \tilde{x}_{i+1}) \cdot J(\tilde{x}_{i+2} - \tilde{x}_{i+1}) = \lambda_i(\boldsymbol{r})$, we obtain the solution (5). Finally, each force $\tilde{f}_i = \sigma\lambda_i(\boldsymbol{r}) \cdot (\boldsymbol{r} - \tilde{x}_i)$ must lie in its friction cone $\tilde{\mathcal{C}}_i$. Due to the homogeneity of the cone $\tilde{\mathcal{C}}_i$ in $\tilde{f}_i$, only the *sign* of $\sigma\lambda_i(\boldsymbol{r})$ matters. Note that $\sigma = 0$, or $\boldsymbol{r} = \tilde{x}_i$ for some i, yield the trivial solution $\tilde{f}_1 = \tilde{f}_2 = \tilde{f}_3 = 0_{2\times 1}$. Hence σ can be either positive or negative, but not zero. Considering both cases for $\mathsf{sgn}(\sigma)$, the region $P_+ \cup P_-$ in (6) is obtained. □

Example: Figure 1 shows two 3-contact arrangements in 3D, together with the friction cones $\mathcal{C}_i$ for $\mu = 0.2$. Figure 2 shows the projections of the contacts $\tilde{x}_i$ onto the horizontal plane, together with the projected friction cones $\tilde{\mathcal{C}}_i$. In Figure 2a the shaded region $P = P_+$ is simply the intersection of the three cones $\tilde{\mathcal{C}}_i$. In Figure 2b the shaded region is $P = P_+ \cup P_-$, where $P_+ = \tilde{\mathcal{C}}_1 \cap \tilde{\mathcal{C}}_2 \cap \tilde{\mathcal{C}}_3$, and P_- is the intersection of $\tilde{\mathcal{C}}_1$ and $\tilde{\mathcal{C}}_2$ with the negative reflection of $\tilde{\mathcal{C}}_3$. In both contact arrangements, the horizontal forces $\tilde{f}_i$ are parametrized by $(\boldsymbol{r}, \sigma)$, such that $\boldsymbol{r} \in P$ and $\sigma \in \mathbb{R}$.
Our next step is to extend the parametrization of the horizontal forces to a parametrization of the full contact forces by the pair $(\boldsymbol{r}, \boldsymbol{\zeta}) \in \mathbb{R}^2 \times \mathbb{R}^3$, where the intermediate parameter σ is eliminated. Recall that $\boldsymbol{r}$ is the planar intersection point of $\tilde{f}_i$. Let l_r be the vertical line in $\mathbb{R}^3$ whose horizontal projection is $\boldsymbol{r}$. A natural choice for parametrizing the vertical component of $\vec{f}_i$ is ζ_i—the vertical distance between the contact x_i and the point where the line of $\vec{f}_i$ intersects the vertical line l_r (Figure 3a). Let $\boldsymbol{\zeta} = (\zeta_1, \zeta_2, \zeta_3)$. We now define Q

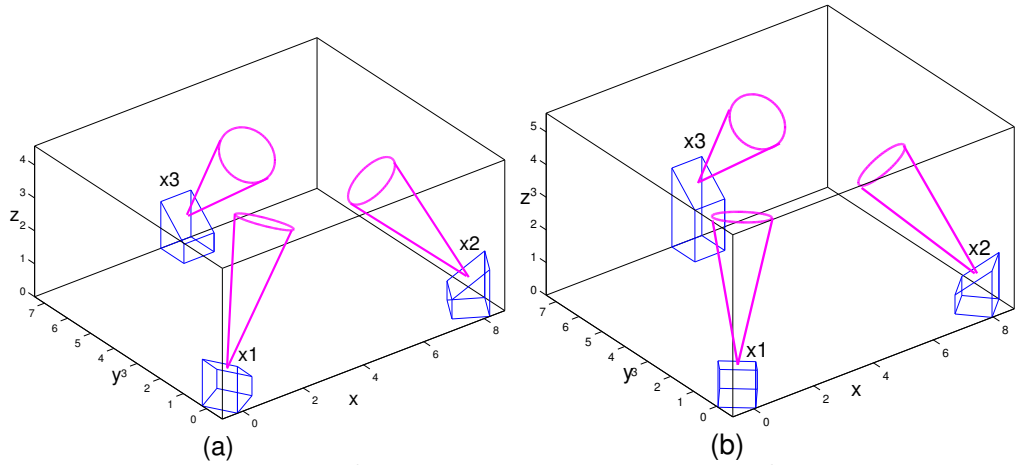

Figure 1: Two three-contact arrangements with $\mu = 0.2$.

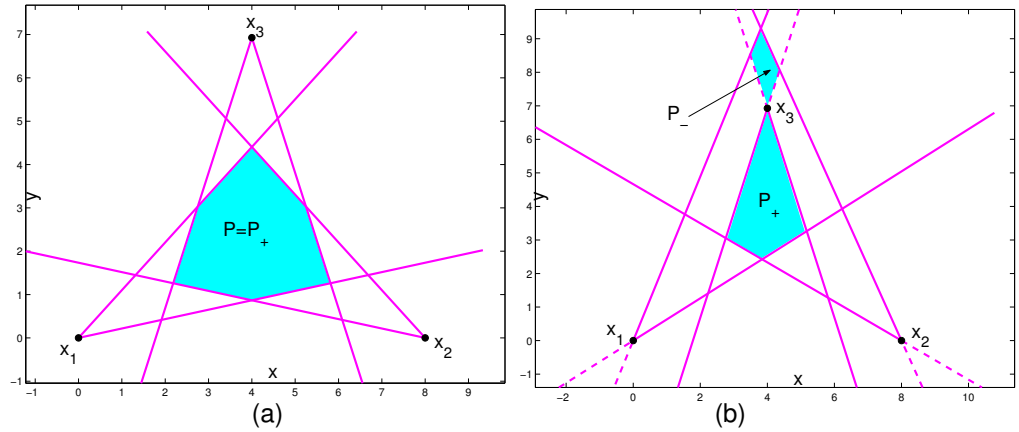

Figure 2: The horizontal projection of the contacts and friction cones, and the resulting region P (shaded).

as the permissible region of $(\boldsymbol{r}, \boldsymbol{\zeta})$ implied by the frictional constraints (2), and analyze its structure. The projection of Q onto the $\boldsymbol{r}$-plane is the polygonal region P defined in (6). Let Π be the vertical prism in $I\!R^3$ whose horizontal cross-section is P. The pair $(\boldsymbol{r}, \zeta_i)$ determine the direction of $\vec{f_i}$. Its permissible region, denoted $\tilde{Q}_i$, is obtained by the intersection of the prism Π and the friction cone $\mathcal{C}_i$ in the physical space (Figure 3b). Therefore, Q is the intersection $Q_1 \cap Q_2 \cap Q_3$, where Q_i is the cylinder obtained by properly lifting $\tilde{Q}_i$ to $(\boldsymbol{r}, \boldsymbol{\zeta})$ space. The following lemma summarizes the parametrization of the contact forces $\vec{f_i}$ by the pair $(\boldsymbol{r}, \boldsymbol{\zeta})$, and formulates the permissible region Q.

Lemma 3.2. *The full contact forces solving equations (4a) and (4b) are parametrized by* $(\boldsymbol{r}, \boldsymbol{\zeta}) \in I\!R^2 \times I\!R^3$ *as follows:*

$$\vec{f_i} = \sigma(\boldsymbol{r}, \boldsymbol{\zeta}) \lambda_i(\boldsymbol{r}) (E(\boldsymbol{r} - \tilde{x}_i) + \zeta_i \boldsymbol{e}) \text{ for } i = 1, 2, 3, \tag{7}$$

where $\lambda_i(\boldsymbol{r}) = (\boldsymbol{r} - \tilde{x}_{i+1}) \cdot J(\tilde{x}_{i+2} - \tilde{x}_{i+1})$, *and* $\sigma(\boldsymbol{r}, \boldsymbol{\zeta}) = 1/(\lambda_1(\boldsymbol{r})\zeta_1 + \lambda_2(\boldsymbol{r})\zeta_2 + \lambda_3(\boldsymbol{r})\zeta_3)$. *Furthermore, in order to satisfy* $\vec{f_i} \in \mathcal{C}_i$, *the parameters* $(\boldsymbol{r}, \boldsymbol{\zeta})$ *must lie within a region* $Q = Q_1 \cap Q_2 \cap Q_3$, *where* Q_i *are defined by:*

$$\begin{aligned} Q_i = \{(\boldsymbol{r}, \boldsymbol{\zeta}) : \boldsymbol{r} \in P \ , \ \sigma(\boldsymbol{r}, \boldsymbol{\zeta}) \lambda_i(\boldsymbol{r}) \zeta_i \geq 0, \text{ and} \\ \sigma(\boldsymbol{r}, \boldsymbol{\zeta}) \lambda_i(\boldsymbol{r}) (E(\boldsymbol{r} - \tilde{x}_i) + \zeta_i \boldsymbol{e})^T B_i (E(\boldsymbol{r} - \tilde{x}_i) + \zeta_i \boldsymbol{e}) \leq 0\}, \text{ for } i = 1, 2, 3. \end{aligned} \tag{8}$$

Proof: As shown in Lemma 3.1, choosing $\tilde{f}_i = \sigma\lambda_i(\boldsymbol{r})(\boldsymbol{r} - \tilde{x}_i)$ satisfies Eq. (4a) for any value of σ. Choosing $f_z^i = \sigma\lambda_i(\boldsymbol{r})\zeta_i$ and substituting into (4b) gives $(\lambda_1(\boldsymbol{r})\zeta_1 + \lambda_2(\boldsymbol{r})\zeta_2 + \lambda_3(\boldsymbol{r})\zeta_3)\sigma = 1$. Therefore $\sigma = 1/(\lambda_1(\boldsymbol{r})\zeta_1 + \lambda_2(\boldsymbol{r})\zeta_2 + \lambda_3(\boldsymbol{r})\zeta_3)$ solves Eq. (4b). It was also shown in Lemma 3.1 that $\boldsymbol{r}$ must lie in P. Since we assumed *upward pointing* contacts, the linear inequalities $n_i \cdot \vec{f}_i \geq 0$ in (3) can be replaced with $f_i^z \geq 0$. Finally, substituting the expression (7) for $\vec{f}_i(\boldsymbol{r}, \boldsymbol{\zeta})$ into the quadratic friction cone constraint in (3) yields the second inequality in (8). □

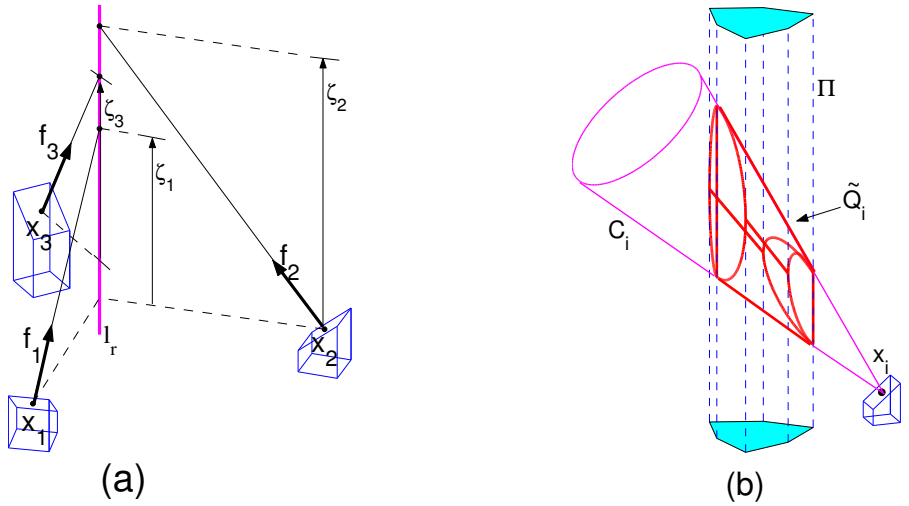

Figure 3: (a) Graphic illustration of ζ_i. (b) The permissible region $\tilde{Q}_i$ in physical space.

3.2 Using the parametrization to characterize $\mathcal{R}$

The three reaction forces are parametrized by the parameters $(\boldsymbol{r}, \boldsymbol{\zeta}) \in Q$, where $Q \subset I\!R^2 \times I\!R^3$ is defined in (8). Recall that the equilibrium condition was decomposed into three equation sets in (4), such that only Eq. (4c) depends on $\tilde{\boldsymbol{x}}$. Using the parametrization (7), Eq. (4c) defines a map $\Phi : Q \to I\!R^2$ from $(\boldsymbol{r}, \boldsymbol{\zeta})$ to the center-of-mass horizontal position $\tilde{\boldsymbol{x}}$ that generates an equilibrium posture, as follows:

$$\begin{aligned}
&\tilde{\boldsymbol{x}} = \Phi(\boldsymbol{r}, \boldsymbol{\zeta}) = \sigma(\boldsymbol{r}, \boldsymbol{\zeta}) \cdot \textstyle\sum_{i=1}^{3} \lambda_i(\boldsymbol{r})[\bar{H}_i(\boldsymbol{r} - \tilde{x}_i) + \bar{h}_i\zeta_i], \\
&\text{where } \lambda_i(\boldsymbol{r}) = (\boldsymbol{r} - \tilde{x}_{i+1}) \cdot J(\tilde{x}_{i+2} - \tilde{x}_{i+1}) \;\;,\;\; \sigma(\boldsymbol{r}, \boldsymbol{\zeta}) = 1/(\lambda_1(\boldsymbol{r})\zeta_1 + \lambda_2(\boldsymbol{r})\zeta_2 + \lambda_3(\boldsymbol{r})\zeta_3) \;\;, \\
&\bar{H}_i = JH_i \;\;,\;\; \bar{h}_i = Jh_i \;\text{,for } i = 1, 2, 3.
\end{aligned} \tag{9}$$

The horizontal cross-section of $\mathcal{R}$ is precisely the image of Q under Φ. However, Φ is highly nonlinear and its image is not easy to compute. In the following, we first approximate the cross-section $\widetilde{\mathcal{R}}$ by formulating a partial set of its candidate boundary curves in explicit closed form. Then we complete the computation by expressing the exact boundary curves as a solution of an implicit high-degree polynomial.

3.3 A Conservative Approximation for $\mathcal{R}$

As stated above, computing the exact image of Q under Φ is not obvious. However, a natural approximation for its boundary curves is the image of the boundary of Q under Φ.

In particular, we are interested in curves on the boundary $\partial Q_1 \cap \partial Q_2 \cap \partial Q_3$, whose projection onto the $\boldsymbol{r}$ plane lies on the boundary of P. The restriction $(\boldsymbol{r}, \boldsymbol{\zeta}) \in \partial Q_1 \cap \partial Q_2 \cap \partial Q_3$ implies that all contact forces lie on the boundary of $\mathcal{C}_i$. Using the quadratic friction constraint in (8), each nonzero ζ_i must satisfy $(E(\boldsymbol{r} - \tilde{x}_i) + \zeta_i \boldsymbol{e})^T B_i (E(\boldsymbol{r} - \tilde{x}_i) + \zeta_i \boldsymbol{e}) = 0$. Solving this quadratic equation for ζ_i gives the relation

$$\begin{aligned} &\zeta_i(\boldsymbol{r}) = \tilde{b}_i^T(\boldsymbol{r} - \tilde{x}_i) \pm \sqrt{(\boldsymbol{r} - \tilde{x}_i)^T \tilde{B}_i (\boldsymbol{r} - \tilde{x}_i)}, \\ &\text{where } \tilde{b}_i = -\tfrac{1}{\boldsymbol{e}^T B_i \boldsymbol{e}} E^T B_i \boldsymbol{e}, \\ &\text{and } \tilde{B}_i = \tfrac{1}{(\boldsymbol{e}^T B_i \boldsymbol{e})^2} E^T B_i [(\boldsymbol{e}\boldsymbol{e}^T) - (\boldsymbol{e}^T B_i \boldsymbol{e}) I_{3\times 3}] B_i E. \end{aligned} \tag{10}$$

Since ζ_i are defined by $\boldsymbol{r}$, which lies on the boundary of P, they form one-dimensional curves on ∂Q. The image of these curves under Φ are closed curves in $I\!R^2$, which are taken as an approximation for the boundary of $\widetilde{\mathcal{R}}$. The following proposition summarizes the computation of the approximate cross-section $\widetilde{\mathcal{R}}$

Proposition 3.3. *A conservative approximation for the region $\widetilde{\mathcal{R}}$ is the convex hull of the following curves, each associated with a single edge of the polygonal region P,*

$$\tilde{\boldsymbol{x}}(s) = \Phi(\boldsymbol{r}(s), \boldsymbol{\zeta}(s)) \;\; s \in [0, 1], \tag{11}$$

where the map Φ is defined in (9), and $\boldsymbol{r}(s), \boldsymbol{\zeta}(s)$ are defined by:

$$\begin{aligned} &\boldsymbol{r}(s) = s\boldsymbol{v}' + (1-s)\boldsymbol{v}'' \\ &\zeta_i(s) = \tilde{b}_i^T(\boldsymbol{r}(s) - \tilde{x}_i) \pm \sqrt{(\boldsymbol{r}(s) - \tilde{x}_i)^T \tilde{B}_i (\boldsymbol{r}(s) - \tilde{x}_i)} \end{aligned} \tag{12}$$

and $\boldsymbol{v}', \boldsymbol{v}''$ are two adjacent vertices of the polygonal region P.

Proof: Recall that we compute the image of Φ only for $\boldsymbol{r}$ on the boundary of P, and ζ_i on the boundary of $\mathcal{C}_i$. Hence $\boldsymbol{r}$ is parametrized by a single parameter s as a convex combination of two adjacent vertices $\boldsymbol{v}'$ and $\boldsymbol{v}''$ of P. Since ζ_i correspond to contact forces on the boundary of the friction cone, they are defined by $\boldsymbol{r}$ as in Eq. (10). Finally, using the convexity of $\widetilde{\mathcal{R}}$ (Lemma 2.1), since the curves $\tilde{\boldsymbol{x}}(s)$ lie in $\widetilde{\mathcal{R}}$, their convex hull also lies in $\widetilde{\mathcal{R}}$. Hence this convex hull gives a conservative approximation for $\widetilde{\mathcal{R}}$. □

Example: Figure 4 shows the approximate $\widetilde{\mathcal{R}}$ for the 3-contact arrangements depicted in Figure 1. For each contact arrangement the polygonal region P and its vertices were computed, then the approximate boundary curves were computed according to Proposition 3.3, resulting in closed curves. In Figure 12a, the boldface closed loop is the Φ-image of the edge of P connecting the vertices v_1 and v_2. All other curves are associated with other edges of P. The convex hull was then taken by adding tangent segments (dashed lines) which were computed numerically. The result is a convex approximation for $\widetilde{\mathcal{R}}$ (shaded region).
The fact that the image of the edges of P do not enclose a convex region is a clear evidence that there are some missing boundary curves, completing the exact boundary of $\widetilde{\mathcal{R}}$. These missing boundary curves correspond to the image of points $\boldsymbol{r}$ in the *interior* of P. The exact computation of these "interior" curves, and consequently the exact computation of $\widetilde{\mathcal{R}}$ is shown in the following.

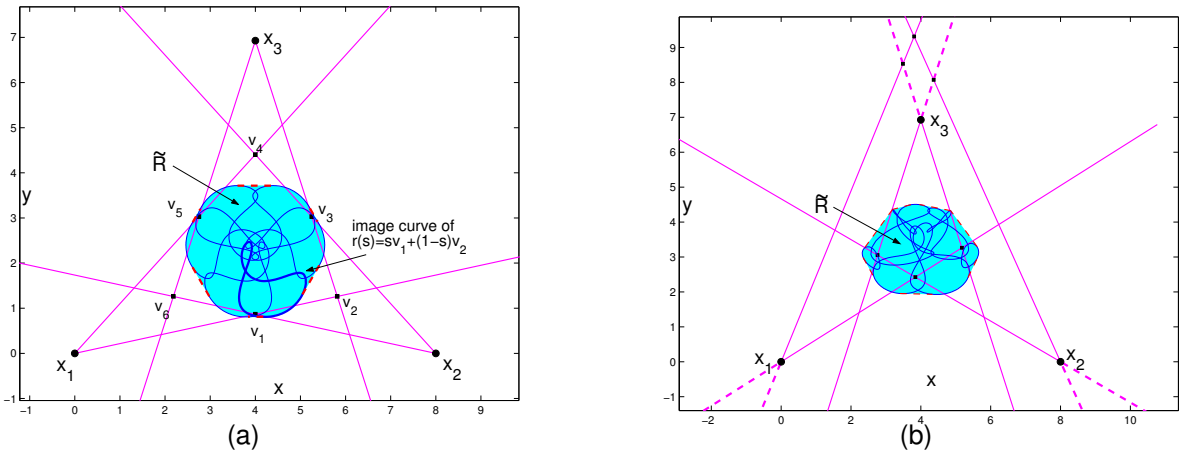

Figure 4: A conservative approximation of $\widetilde{\mathcal{R}}$ (shaded) and the boundary curves generated by the edges of the polygon P, for the contact arrangements depicted in Figure 1.

3.4 Exact Computation of $\mathcal{R}$

We now complete the computation of the exact boundary of $\widetilde{\mathcal{R}}$. Recall the definition of the region $Q = Q_1 \cap Q_2 \cap Q_3$ of $(\boldsymbol{r}, \boldsymbol{\zeta})$ corresponding to contact forces $\vec{f}_i$ lying within the friction cones $\mathcal{C}_i$ for $i = 1, 2, 3$. The boundary curves of the image of Q under Φ are image of critical curves of Φ in Q, on which the Jacobian matrix $D\Phi$ loses full rank. The critical curves can be classified into four classes from type-0 to type-3, where type-n curves lie on a submanifold of Q corresponding to contact forces such that n forces lie on the boundary of their friction cones. The following proposition formulates all types of critical curves as solutions of implicit equations.

Proposition 3.4. *Let $\Phi : Q \to \mathbb{R}^2$ be the map of $(\boldsymbol{r}, \boldsymbol{\zeta})$ to $\tilde{x}$. The four types of critical points of Φ on Q are formulated as follows:*
Type-0 critical points: *Critical points lying in the interior of Q do not exist for any non-planar contact arrangement.*
Type-1 critical points: *Type-1 Critical points have $\boldsymbol{r}$-component that lie on straight lines passing through two projected contact points $\tilde{x}_i$ and $\tilde{x}_j$, as long as this line intersects the polygonal region P.*
Type-2 critical points: *There are two cases of Type-2 critical points:*
a. Points at which $\boldsymbol{r} = \tilde{x}_i$, as long as the friction cone $\mathcal{C}_i$ contains the upward direction $\boldsymbol{e}$.
b. Lines with $\boldsymbol{r}, \zeta_2$ and ζ_3 fixed at $\boldsymbol{r}^*, \zeta_2^*$ and ζ_3^*, while ζ_1 varies freely. (The contacts' indices can be arbitrarily permuted). The fixed values of ζ_2 and ζ_3 are defined by $\boldsymbol{r}^*$, as in Eq. (10). The fixed value of $\boldsymbol{r}$ is the solution of the two implicit equations:

$$\det[M_2(\boldsymbol{r})] = 0, \text{ and } \det\left[M_2(\boldsymbol{r}) \begin{pmatrix} 0 \\ 1 \end{pmatrix} \quad \bar{h}_1 - \boldsymbol{u}(\boldsymbol{r})\right] = 0, \tag{13}$$

where $M_2(\boldsymbol{r})$ and $\boldsymbol{u}(\boldsymbol{r})$ are obtained by composition of the following functions:

$$
\begin{aligned}
M_2(\boldsymbol{r}) &= \Big[\textstyle\sum_{j=2}^{3}\lambda_j(\boldsymbol{r})\zeta_j(\boldsymbol{r})\Big]\,\big[\textstyle\sum_{i=1}^{3}\bar{H}_i\lambda_i(\boldsymbol{r})+\bar{H}_i(\boldsymbol{r}-\tilde{x}_i)\lambda_i'(\boldsymbol{r})+\sum_{i=2}^{3}\bar{h}_i(\lambda_i(\boldsymbol{r})\zeta_i'(\boldsymbol{r})+\lambda_i'(\boldsymbol{r})\zeta_i(\boldsymbol{r}))\big]\\
&\quad-\big[\textstyle\sum_{i=1}^{3}\lambda_i\bar{H}_i(\boldsymbol{r}-\tilde{x}_i)+\sum_{i=2}^{3}\bar{h}_i\lambda_i(\boldsymbol{r})\zeta_i(\boldsymbol{r}))\big]\,\Big[\textstyle\sum_{j=2}^{3}\lambda_j(\boldsymbol{r})\zeta_j'(\boldsymbol{r})+\lambda_j'(\boldsymbol{r})\zeta_j(\boldsymbol{r})\Big]\\
\boldsymbol{u}(\boldsymbol{r}) &= \tfrac{1}{\lambda_2(\boldsymbol{r})\zeta_2(\boldsymbol{r})+\lambda_3(\boldsymbol{r})\zeta_3(\boldsymbol{r})}J\,\big[\textstyle\sum_{i=1}^{3}[\bar{H}_i\lambda_i(\boldsymbol{r})(\boldsymbol{r}-\tilde{x}_i)]+\bar{h}_2\lambda_2(\boldsymbol{r})\zeta_2(\boldsymbol{r})+\bar{h}_3\lambda_3(\boldsymbol{r})\zeta_3(\boldsymbol{r})\big]\\
\lambda_i(\boldsymbol{r}) &= (\boldsymbol{r}-\tilde{x}_{i+1})\cdot J(\tilde{x}_{i+2}-\tilde{x}_{i+1})\\
\zeta_i(\boldsymbol{r}) &= \tilde{b}_i^T(\boldsymbol{r}-\tilde{x}_i)\pm\sqrt{(\boldsymbol{r}-\tilde{x}_i)^T\tilde{B}_i(\boldsymbol{r}-\tilde{x}_i)}\\
\lambda_j'(\boldsymbol{r}) &= (\tilde{x}_{i+2}-\tilde{x}_{i+1})^TJ^T\\
\zeta_i'(\boldsymbol{r}) &= \tilde{b}_i^T\pm\tfrac{1}{\sqrt{(\boldsymbol{r}-\tilde{x}_i)^T\tilde{B}_i(\boldsymbol{r}-\tilde{x}_i)}}(\boldsymbol{r}-\tilde{x}_i)^T\tilde{B}_i
\end{aligned}
\tag{14}
$$

Type-3 critical points: *There are two cases of Type-3 critical points:*
a. Curves of $(\boldsymbol{r},\boldsymbol{\zeta})\in\partial Q_1\cap\partial Q_2\cap\partial Q_3$ such that $\boldsymbol{r}\in\partial P$. These one-dimensional curves are already considered in the approximation stage, and are formulated in closed form in Eq. (12) in Proposition 3.3.
b. Curves of $(\boldsymbol{r},\boldsymbol{\zeta})\in\partial Q_1\cap\partial Q_2\cap\partial Q_3$ such that $\boldsymbol{r}$ is the solution of the implicit equation $\det[M_3(\boldsymbol{r})]=0$, *where $M_3(\boldsymbol{r})$ is obtained by composition of the following functions:*

$$
\begin{aligned}
M_3(\boldsymbol{r}) &= \textstyle\sum_{i=1}^{3}\{[(H_i(\boldsymbol{r}-\tilde{x}_i)+h_i\zeta_i(\boldsymbol{r}))\lambda_i'(\boldsymbol{r})+\lambda_i(\boldsymbol{r})(H_i+h_i\zeta_i'(\boldsymbol{r}))][\textstyle\sum_{j=1}^{3}\lambda_j(\boldsymbol{r})\zeta_j(\boldsymbol{r})]\\
&\quad-\lambda_i(\boldsymbol{r})(H_i(\boldsymbol{r}-\tilde{x}_i)+h_i\zeta_i(\boldsymbol{r}))[\textstyle\sum_{j=1}^{3}\lambda_j(\boldsymbol{r})\zeta_j'(\boldsymbol{r})+\lambda_j'(\boldsymbol{r})\zeta_j(\boldsymbol{r})]\}\\
\lambda_i(\boldsymbol{r}) &= (\boldsymbol{r}-\tilde{x}_{i+1})\cdot J(\tilde{x}_{i+2}-\tilde{x}_{i+1})\\
\zeta_i(\boldsymbol{r}) &= \tilde{b}_i^T(\boldsymbol{r}-\tilde{x}_i)\pm\sqrt{(\boldsymbol{r}-\tilde{x}_i)^T\tilde{B}_i(\boldsymbol{r}-\tilde{x}_i)}\\
\lambda_j'(\boldsymbol{r}) &= (\tilde{x}_{i+2}-\tilde{x}_{i+1})^TJ^T\\
\zeta_i'(\boldsymbol{r}) &= \tilde{b}_i^T\pm\tfrac{1}{\sqrt{(\boldsymbol{r}-\tilde{x}_i)^T\tilde{B}_i(\boldsymbol{r}-\tilde{x}_i)}}(\boldsymbol{r}-\tilde{x}_i)^T\tilde{B}_i,\\
&\text{where } \tilde{b}_i \text{ and } \tilde{B}_i \text{ are defined in (12).}
\end{aligned}
\tag{15}
$$

Moreover, in the special case where all the contacts are located at equal heights, critical curves of type-2b are degenerate, and are not necessary for computation of the boundary.

The full proof appears in the Appendix, and its outline is as follows. First, recall that criticality conditions also hold under change of coordinates. Second, notice that type-1, type-2 and type-3 curves lie in submainfolds of Q, whose dimensions are 4,3 and 2 respectively. Therefore, for each possible type we choose a reduced set of new coordinates, and express the restriction $\bar{\Phi}$ of Φ to the corresponding sumbmanifold of Q with the new coordinates. Then we explicitly compute the Jacobian $D\bar{\Phi}$, and formulate the conditions for its rank deficiency.

We have formulated all the critical curves in $\boldsymbol{r}$-space, whose Φ-image are candidate boundary curves of $\tilde{\mathcal{R}}$. In order to complete the computation, one needs to find these curves, and compute their associated image under Φ. This results in a planar arrangement of candidate boundary curves in $\tilde{x}$-plane. Finally, the actual boundary consists of the "outmost" curves,

and can be found visually, or by simply taking the convex hull of all curves. The following corollary summarizes these concluding steps.

Corollary 3.5. *Given a solid body $\mathcal{B}$ supported by three frictional contacts in a 3D gravitational field, the center-of-mass feasible equilibrium region is a vertical prism, whose horizontal cross-section can be computed by the following steps:*

1. *If the friction cone $\mathcal{C}_i$ contains the vertical direction $\boldsymbol{e}$, then the point $\tilde{\boldsymbol{x}} = \tilde{x}_i$ is a candidate boundary of $\widetilde{\mathcal{R}}$, for $i = 1, 2, 3$.*

2. *If any of the line segments $\tilde{x}_i - \tilde{x}_j$ intersect the polygonal region P, compute the corresponding line segment in $\tilde{\boldsymbol{x}}$-plane, associated with two active contacts exerting forces only in the vertical plane containing $\tilde{x}_i$ and $\tilde{x}_j$, using the planar analysis detailed in [18].*

3. *If the contacts are not located at equal heights, compute type-2b critical curves as formulated in Eq. (13). The Φ-image of these curves, obtained by substitution into Eq. (9), consists of additional candidate boundary curves.*

4. *Compute the approximate boundary curves formulated in Proposition 3.3. These candidate boundary curves are the Φ-image of type-3a critical curves.*

5. *Compute type-3b critical curves, which are solutions of the implicit equation* $\det[M_3(\boldsymbol{r})] = 0$ *defined in Eq.(15). The Φ-image of these curves, obtained by substitution into Eq. (9), consists of additional candidate boundary curves.*

6. *Finally, The convex hull enclosing all the obtained curves is the cross-section $\widetilde{\mathcal{R}}$.*

The implicit representation of type-2a and type-3a critical curves are highly nonlinear, and by choosing a particular coordinate system, they can be rearranged and simplified to polynomials of degree 24 in $\boldsymbol{r}$, which do not have analytical solutions. However, since $\boldsymbol{r}$ lies in P, which is generally bounded, the critical points can be computed by numerical search for all zeros of high-order polynomial within a bounded two-dimensional region. In the following example, we used a numerical search to find the critical curves and compute the exact boundary of $\widetilde{\mathcal{R}}$.

Example: Figure 5a shows the $\boldsymbol{r}$-component of type-3b critical curves for the 3-contact arrangement depicted in Figure 1a. Recall that the $\boldsymbol{r}$-component of type-3a critical curves is simply the boundary of the polygonal region P. Figure 6a shows in $\tilde{\boldsymbol{x}}$-plane the Φ-image of type-3a critical curves (dashed), and of type-3b critical curves (solid). Notice both types of candidate boundary curves are required to enclose a convex region, which is the exact cross-section $\widetilde{\mathcal{R}}$ (shaded region). Notice that since in this arrangement the contacts are located at equal heights, type-2b critical curves do not contribute any associated boundary curves, as stated in Proposition 3.4. Figure 5b shows the $\boldsymbol{r}$-component of type-3b critical curves for the 3-contact arrangement depicted in Figure 1b (solid). The $\boldsymbol{r}$-component of type-2b critical curves are isolated points, also shown in Figure 5b. Some of the points are associated with type-2b critical curves of ζ_1 free (marked by $'\times'$), and others are associated with type-2b critical curves of ζ_2 free (marked by $'+'$). Figure 6b shows in $\tilde{\boldsymbol{x}}$-plane the Φ-image of type-3a critical curves (dashed), of type-3b critical curves (solid) and of type-2b

critical curves (dotted line segments, only those contributing to the actual boundary are drawn), for the 3-contact arrangement depicted in Figure 1b. The enclosed convex region is the exact cross-section $\widetilde{\mathcal{R}}$ (shaded).

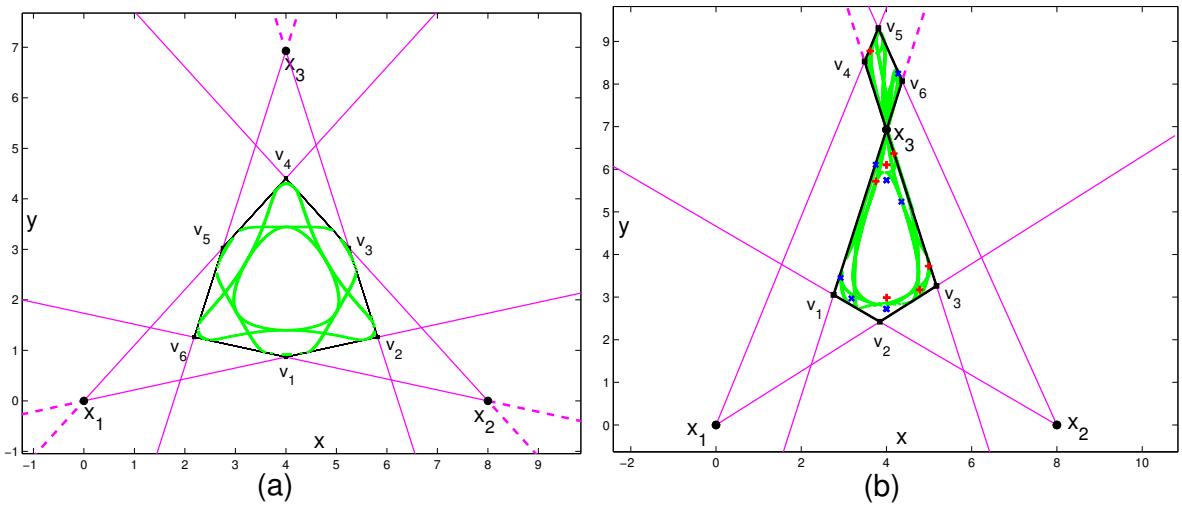

Figure 5: Critical curves in $\boldsymbol{r}$-plane for the contact arrangements depicted in Figure 1.

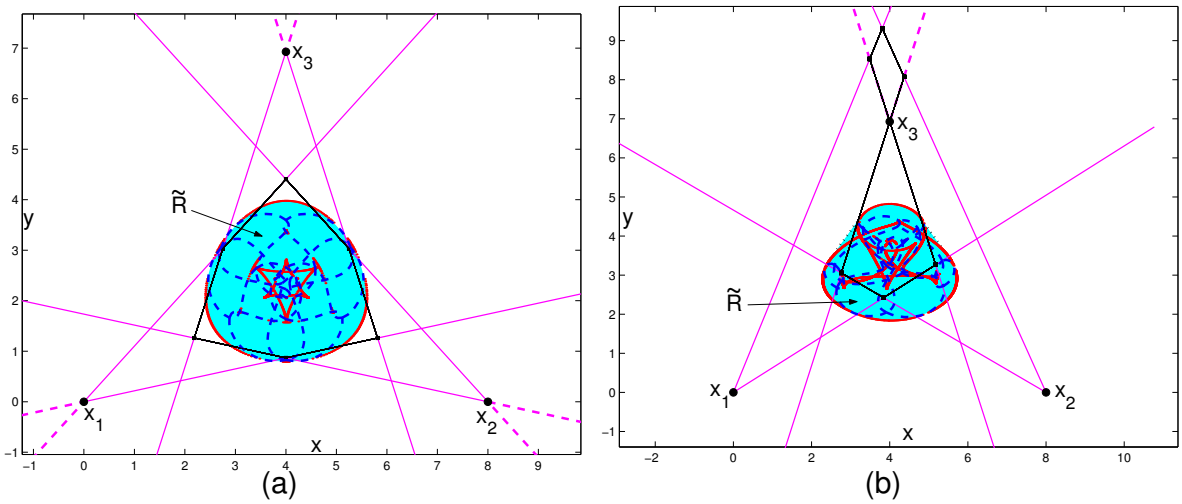

Figure 6: Exact boundary of $\widetilde{\mathcal{R}}$ for the contact arrangements depicted in Figure 1.

4 Postures Computation by Projection Approach

In this section we extend to a general number $k \geq 3$ of contacts, and show that the cross-section $\widetilde{\mathcal{R}}$ can be obtained by projecting a region in a high-dimensional space onto a two-dimensional plane. First, we define the *equilibrium space* — an abstract high-dimensional space combining center-of-mass locations and contact forces satisfying equilibrium condition. Then we show that frictional constraints define a feasible region in the equilibrium space, whose projection onto $\tilde{\boldsymbol{x}}$-plane gives the feasible region cross-section $\widetilde{\mathcal{R}}$. Next, we formulate the conditions for silhouette curves whose projection are candidate boundary curves of $\widetilde{\mathcal{R}}$ as a system of implicit polynomial equations. Finally, we provide an approximate solution by using polyhedral approximation of the frictional constraints, and applying an efficient projection algorithm presented by [21]. The approximated region is demonstrated graphically, and compared with the results obtained by the parametrization approach for the 3-contact case.

4.1 Definition of the Equilibrium Space

Consider a solid body $\mathcal{B}$ supported by k frictional contacts in three dimensional gravitational field. Define $\vec{f} = (\vec{f_1} \cdots \vec{f_k}) \in I\!R^{3k}$ as the combined forces vector. Scaling force units such that $\|\vec{f_g}\| = 1$, the equilibrium condition (1) can be written in matrix form as

$$G\vec{f} = T\tilde{x} + u_o,$$
$$\text{where } G = \begin{pmatrix} I & \cdots & I \\ [x_1\times] & \cdots & [x_k\times] \end{pmatrix} \ , \ T = \begin{pmatrix} 0_{3\times 2} \\ EJ^TE^T \end{pmatrix} \ , \ u_o = \begin{pmatrix} \boldsymbol{e} \\ \vec{0} \end{pmatrix}, \tag{16}$$

and $\tilde{x}$ is the horizontal projection of the center-of-mass location. For number of contacts $k \geq 3$, the static response is indeterminate of degree $m = 3(k-2)$. Therefore, the static forces $\vec{f_i}$ can be expressed by $\boldsymbol{v} \in I\!R^m$ and $\tilde{\boldsymbol{x}} \in I\!R^2$, as

$$\vec{f} = M_v\boldsymbol{v} + M_x\tilde{\boldsymbol{x}} + \boldsymbol{v}_o, \tag{17}$$

where $M_v \in I\!R^{3k\times m}$ is a matrix whose columns form a basis of the nullspace of G, $M_x = G^\dagger T$ and $\boldsymbol{v}_o = G^\dagger u_o$, where $G^\dagger$ is the pseudo-inverse of G. The pair $(\tilde{\boldsymbol{x}}, \boldsymbol{v})$ parametrizes all center-of-mass locations and contact forces satisfying the equilibrium condition (16). The frictional constraints (3) can be written as:

$$\vec{f}\cdot\bar{n}_i \geq 0 \ , \ \vec{f}^T\bar{B}_i\vec{f} \geq 0 \ , \ i = 1\ldots k \tag{18}$$

where $\bar{n}_i$ and $\bar{B}_i$ are n_i and B_i properly augmented in a column vector and a block-diagonal matrix respectively. Substituting the expression for $\vec{f}$ in (17) into the inequality constraints (18), gives $2k$ inequalities in $(\tilde{\boldsymbol{x}}, \boldsymbol{v})$. These inequalities define a feasible region $\mathcal{S}$ in the equilibrium space of $(\tilde{\boldsymbol{x}}, \boldsymbol{v})$:

$$\begin{aligned} \mathcal{S} = \{(\tilde{\boldsymbol{x}}, \boldsymbol{v}) : \ & \bar{n}_i\cdot(M_v\boldsymbol{v} + M_x\tilde{\boldsymbol{x}} + \boldsymbol{v}_o) \geq 0, \\ & (M_v\boldsymbol{v} + M_x\tilde{\boldsymbol{x}} + \boldsymbol{v}_o)^T\bar{B}_i(M_v\boldsymbol{v} + M_x\tilde{\boldsymbol{x}} + \boldsymbol{v}_o) \geq 0 \text{ , for } i = 1\ldots k\} \end{aligned} \tag{19}$$

The boundary of $\mathcal{S}$ is a stratified set consisting of k hyperplanes, k quadratic hypersurfaces, and all their intersection manifolds. The projection of $\mathcal{S}$ onto the $\tilde{\boldsymbol{x}}$-plane is precisely the cross-section $\widetilde{\mathcal{R}}$ of the center-of-mass feasible region.

4.2 Projecting $\mathcal{S}$ onto $\tilde{x}$-plane

We now characterize the the boundary curves of $\widetilde{\mathcal{R}}$, and express them as solutions of systems of quadratic polynomials in $(\tilde{\boldsymbol{x}}, \boldsymbol{v})$. The boundary curves of $\widetilde{\mathcal{R}}$ are projection of *silhouette curves* of $\mathcal{S}$. The following theorem which characterizes the silhouette curves, is an adaptation of standard results to our purposes (e.g. [3, p. 102]).

Theorem 1 (Silhouette Theorem). *Let* $\Pi : I\!R^{m+2} \to I\!R^2$ *be the coordinate projection* $\Pi(\tilde{\boldsymbol{x}}, \boldsymbol{v}) = \tilde{\boldsymbol{x}}$. *Let* $\mathcal{S} = \{(\tilde{\boldsymbol{x}}, \boldsymbol{v}) \in I\!R^{2+m} : \Psi_1(\tilde{\boldsymbol{x}}, \boldsymbol{v}) \leq 0, \ldots, \Psi_{2k}(\tilde{\boldsymbol{x}}, \boldsymbol{v}) \leq 0\}$. *Then* $\Pi(\mathcal{S})$ *is a two-dimensional region bounded by the projection of the silhouette curves of* $\mathcal{S}$, *consisting of critical points of* Π *on the boundary of* $\mathcal{S}$. *Moreover, the silhouette curves consist of points* $(\tilde{\boldsymbol{x}}, \boldsymbol{v}) \in \mathcal{S}$ *on which the gradients* $\{\nabla_v \Psi_{i_1}(\tilde{\boldsymbol{x}}, \boldsymbol{v}), \ldots, \nabla_v \Psi_{i_n}(\tilde{\boldsymbol{x}}, \boldsymbol{v})\}$ *positively span the zero vector, where* $\Psi_{i_1}, \ldots, \Psi_{i_n}$ *are the constraints that vanish at* $(\tilde{\boldsymbol{x}}, \boldsymbol{v})$.

We now provide a characterization of the silhouette curves of $\mathcal{S}$ by using the Silhouette Theorem. At this stage, we focus on silhouette curves associated with contact forces that are all active, hence all contact forces satisfy $n_i \cdot \vec{f_i} > 0$ for $i = 1 \ldots k$. The silhouette curves can be classified into k types, where type-n curves consist of points $(\tilde{\boldsymbol{x}}, \boldsymbol{v}) \in \partial\mathcal{S}$ on which n of the quadratic inequalities in (19) vanish. Therefore, such curves lie on a submanifold of dimension $m + 2 - n$. Let $i_1 \ldots i_n$ be the indices of the vanishing constraints. Using the Silhouette Theorem, the silhouette condition states that the gradient vectors $\{\nabla_v \Psi_{i_j} = M_v^T \bar{B}_i (M_v \boldsymbol{v} + M_x \tilde{\boldsymbol{x}} + \boldsymbol{v}_o) \quad j = 1 \ldots n\}$ positively span the zero vector. Since $n < m$, the matrix $M_n(\tilde{\boldsymbol{x}}, \boldsymbol{v}) = [\nabla_v \Psi_{i_1}, \ldots, \nabla_v \Psi_{i_n}]$ must be rank-deficient. This implies that $m - n + 1$ determinants of $n \times n$ sub-matrices of $M_n(\tilde{\boldsymbol{x}}, \boldsymbol{v})$ must vanish. Therefore, the n-type silhouette curves associated with the indices $i_1 \ldots i_n$ are defined as the intersection of n quadratic hypersurfaces $\Psi_{i_j} = 0$, $j = 1 \ldots n$, and $m - n + 1$ determinants of square sub-matrices of $M_n(\tilde{\boldsymbol{x}}, \boldsymbol{v})$ that vanish. This amounts to a solution of generically-independent $m - 1$ scalar equations in $I\!R^2 \times I\!R^m$, which gives a one-dimensional curve. Notice that some of the solutions are redundant, because they do not satisfy the condition of *positive* span. For a given solution $(\tilde{\boldsymbol{x}}, \boldsymbol{v})$, checking the positive span condition can be done by solving a simple linear program.

In order to treat the case where some of the contact forces are inactive, one needs to repeat the steps detailed above for all possible k'-tuples of contacts, where $k' = 1 \ldots k - 1$. The computation of all the silhouette curves results in a planar arrangement of candidate boundary curves in $\tilde{x}$-plane. Finally, the actual boundary consists of the "outmost" curves, and can be found visually, or by simply taking the convex hull of all curves. The following corollary summarizes the computation of $\widetilde{\mathcal{R}}$ using the projection approach.

Corollary 4.1. *Given a solid body $\mathcal{B}$ supported by three frictional contacts in a 3D gravitational field, the center-of-mass feasible equilibrium region is a vertical prism, whose horizontal cross-section can be computed by the following steps:*

for $i = 1 \dots k$
  if the cone $\mathcal{C}_i$ *contains the upward direction* $\boldsymbol{e}$,
  the point $\tilde{x}_i$ *is a candidate boundary of*$\widetilde{\mathcal{R}}$.
for all pairs $i, j \in \{1 \dots k\}$ *such that* $i \neq j$
  Define V *as the vertical plane passing through* $\tilde{x}_i$ *and* $\tilde{x}_j$.
  if V *has non-degenerate intersection with the cones* $\mathcal{C}_i$ *and* $\mathcal{C}_j$,
  compute candidate curve as the horizontal projection
  of the associated 2D feasible equilibrium region,
  which can be computed using the planar methods detailed in [18].
for $k' = 3 \dots k$
  for each possible k'*-tuple of active contacts*
    formulate the equilibrium condition (16) associated with the active contacts
    Construct the corresponding $(\tilde{\boldsymbol{x}}, \boldsymbol{v})$ *parametriztion (17),*
    where $\boldsymbol{v}$ *is of dimension* $m' = 3(k' - 2)$.
    for $n = 1 \dots k'$
      for each possible index subset $i_1 \dots i_n$ *of the active contacts*
        Construct the $m' \times n$ *matrix* $M_n(\tilde{\boldsymbol{x}}, \boldsymbol{v}) = [\nabla_v \Psi_{i_1}, \dots, \nabla_v \Psi_{i_n}]$,
        where $\nabla_v \Psi_{i_j} = M_v^T \bar{B}_i (M_v \boldsymbol{v} + M_x \tilde{\boldsymbol{x}} + \boldsymbol{v}_o)$.
        compute candidate curve, which is the $\tilde{\boldsymbol{x}}$*-component solution of the system:*
          $(M_v \boldsymbol{v} + M_x \tilde{\boldsymbol{x}} + \boldsymbol{v}_o)^T \bar{B}_{i_j} (M_v \boldsymbol{v} + M_x \tilde{\boldsymbol{x}} + \boldsymbol{v}_o) = 0$ *, for* $j = 1 \dots n$
          $\det M_j(\tilde{\boldsymbol{x}}, \boldsymbol{v}) = 0$ *, for* $j = 1 \dots m' - n + 1$
        where M_j *is the square matrix obtained by taking rows* j *to* $j + m - 1$ *of* $M_n(\tilde{\boldsymbol{x}}, \boldsymbol{v})$.
Finally, $\widetilde{\mathcal{R}}$ *is the convex hull enclosing all the candidate curves.*

The projection approach provides implicit characterization of all candidate boundary curves, for any number of frictional contacts. However, it is not practically applicable, even for small number of contacts, because of the following reasons. First, the number of candidate curves grows as fast as $k!$ due to the combinatorial character of index permutations. Second, the maximum total degree of the polynomial systems, grows as fast as $2^k \cdot k^{2k-5}$. For example, five contacts arrangement requires computation of 176 candidate curves represented by systems of polynomial equations, with maximum total degree of 10^5. Moreover, applying dialytic elimination methods [23] for eliminating $\boldsymbol{v}$ and obtaining a single polynomial in $\tilde{\boldsymbol{x}}$, results in a highly complicated polynomial of higher degree, with redundant solutions. In the following, we show that even though the projection approach is impractical for exact computation, it naturally leads to an efficient approximation, when the quadratic friction cones are replaced with circumscribed polyhedra.

4.3 Approximate Solution Using Linear Constraints

We now present an approximate solution using polyhedral approximation of the quadratic frictional constraints, and applying an efficient algorithm for projection of a high-dimensional convex polytope onto a lower dimensional space. First, we formulate the approximation of

friction cones by n-sided polyhedra. Then we represent the approximate linear constraint in the equilibrium space and derive the approximate feasible region $\mathcal{S}'$. Finally, we use the efficient algorithm presented by [21] for projecting $\mathcal{S}'$ onto $\tilde{\boldsymbol{x}}$-space.

The exact friction cone in 3D can be approximated by an n-sided polyhedron, such that the quadratic constraint (2) is replaced with n linear constraints. The approximate polyhedron $\mathcal{C}'_i$ is defined by

$$\begin{aligned}\mathcal{C}'_i = \{\vec{f_i} : &(\sin\theta_{j+1} - \sin\theta_j)(\vec{f_i}\cdot s_i) \\ &+(\cos\theta_j - \cos\theta_{j+1})(\vec{f_i}\cdot t_i) \le \beta(\vec{f_i}\cdot n_i)\ ,\ j = 1\ldots n\},\end{aligned} \tag{20}$$

where $\theta_j = \frac{2\pi j}{n}$, $\beta = \mu\sin\left(\frac{2\pi}{n}\right)$, μ is the coefficient of friction, and (s_i, t_i, n_i) is a right-handed orthonormal frame of two unit tangents and an outward unit normal at x_i. The linear constraints can be written in matrix form as $A_i\vec{f_i} \le 0$, where

$$A_i = \begin{pmatrix} \sin\theta_2 - \sin\theta_1 & \cos\theta_1 - \cos\theta_2 & -\beta \\ \vdots & \vdots & \vdots \\ \sin\theta_{n+1} - \sin\theta_n & \cos\theta_n - \cos\theta_{n+1} & -\beta \end{pmatrix} \begin{pmatrix} s_i & t_i & n_i \end{pmatrix}^T.$$

Using the equilibrium space parametrization (17), the approximated feasible region in $(\tilde{\boldsymbol{x}}, \boldsymbol{v})$ space is the convex polytope defined by

$$\mathcal{S}' = \{(\tilde{\boldsymbol{x}}, \boldsymbol{v}) : \quad \bar{A}_i(M_v\boldsymbol{v} + M_x\tilde{\boldsymbol{x}} + \boldsymbol{v}_o) \le 0,\ \text{, for } i = 1\ldots k\} \tag{21}$$

Where $\bar{A}_i$ is a proper augmentation of A_i in a block-diagonal matrix of dimensions $kn \times 3k$. The approximation of $\widetilde{\mathcal{R}}$ now reduces to computation of the convex polygon $\widetilde{\mathcal{R}}'$ obtained by projecting $\mathcal{S}'$ onto $\tilde{\boldsymbol{x}}$-plane. This is a classical problem, which is widely explored in computational geometry literature (e.g. [6, 8]). In the following examples, we implemented an adapted version of the efficient contour-tracking algorithm proposed by Ponce et. al. for projection of a high-dimensional convex polytope onto a lower dimensional space, in the context of grasp planning. According to the analysis in [21], the algorithm solves a sequence of linear programs, and runs in $O(nkt)$ time, where t is the number of edges in the resulting polygon.

Example: Figure 7 shows the polygonal approximation $\widetilde{\mathcal{R}}'$ (shaded region) compared with the exact boundary of $\widetilde{\mathcal{R}}$ (dashed) for the 3-contact arrangements depicted in Figure 1. The friction cones were approximated by 6-sided polyhedra.

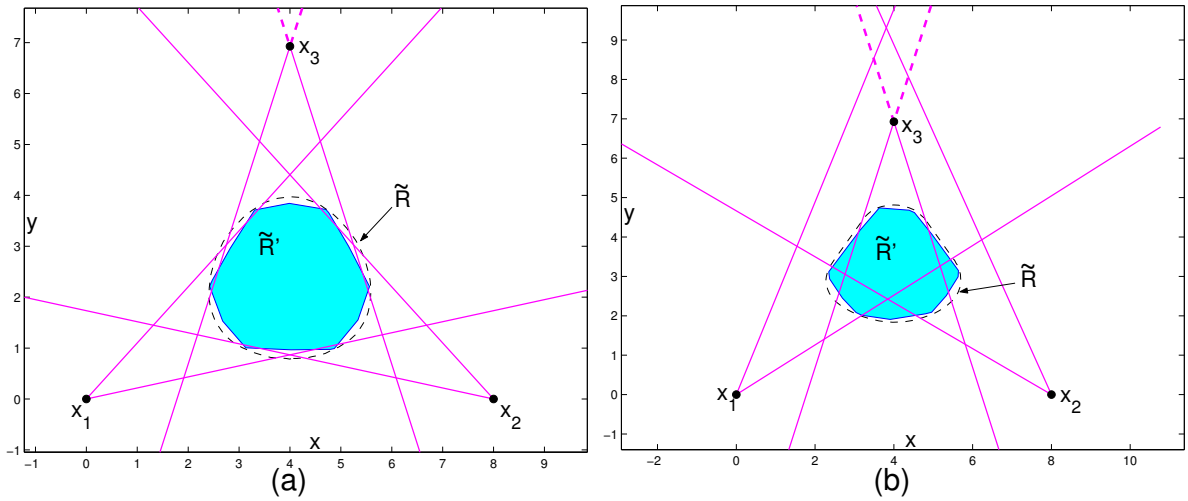

Figure 7: Polygonal approximation $\widetilde{\mathcal{R}}'$ and the exact boundary of $\widetilde{\mathcal{R}}$ (dashed) for the contact arrangements depicted in Figure 1.

5 Conclusion

We have characterized equilibrium postures in 3D arrangement of multiple frictional contacts under gravity. First, we have shown that the center-of-mass feasible equilibrium region $\mathcal{R}$ is a vertical convex prism. In the three-contact case, we defined a natural parametrization of the indeterminate contact forces by five scalar parameters, and derived a closed-form approximation for the boundary of $\mathcal{R}$. Then we expressed the exact boundary as a solution of a high-order polynomial, and provided graphical examples. In the multiple-contact case, we formulated the feasible region as the projection of a high-dimensional region, derived an efficient polyhedral approximation of $\mathcal{R}$, which was demonstrated graphically. The methods developed in this work can serve as a theocratical basis towards 3D locomotion planning on rough terrain.

We now briefly discuss three possible directions of future research. First, the 3-contacts critical curves were formulated as solutions of complicated algebraic equations, and lack a simple graphical characterization. A deeper investigation of the fundamental nature of the criticality condition could provide some graphical insights that would simplify the computation, and may also be helpful in generalizing the parametrization approach to multiple contacts.

Second, the feasible equilibrium region was computed while considering the single load of gravitational forces. However, in practice, one must consider postures which are *robust* with respect to a given neighborhood of disturbance wrenches. Generalizing the characterization of *robust equilibrium* in [18] to three-dimensional environments is still an open problem, subject to current research.

Finally, one must recall that the feasible equilibrium condition is only based on *static* response. In order to select a desired posture, one must also consider its *dynamic stability*, and check the dynamic response at the contacts under small perturbations. A key feature in rigid body dynamics under Coulomb's friction assumption is the *dynamic ambiguity*, where the dynamic response has multiple non-static solutions [11],[22],[14]. In the two-dimensional case, Or and Rimon [17] used the *strong stability* criterion defined by Trinkle et. al. [19]

to characterize 2D postures. Therefore, an additional open problem is generalization of the dynamic analysis to characterize stable 3D postures.

References

[1] A. Bicchi. On the closure properties of robotic grasping. *The International Journal of Robotics Research*, 14(4):319–334, Aug. 1995.

[2] T. Bretl, S. Rock, and J.C. Latombe. Motion planning for a three-limbed climbing robot in vertical natural terrain. In *IEEE Int. Conf. on Robotics and Automation*, pages 2946–2953, 2003.

[3] J. F. Canny. *The complexity of robot motion planning.* MIT Press, Cambridge, MA, 1988.

[4] M. A. Erdmann. An exploration of nonprehensile two-palm manipulation. *The International Journal of Robotics Research*, 17(5), 1998.

[5] Li Han, J.c. Trinkle, and Z.X. Li. Grasp analysis as linear matrix inequality problems. *IEEE Transactions on Robotics and Automation*, 16(6):663–674, 2000.

[6] J. N. Hooker. Logical inference and polyhedral projection. In *Computer Science Logic, 5th Workshop, CSL '91, Proceedings*, pages 184–200, 1991.

[7] R. D. Howe, I. Kao, and M. R. Cutkosky. The sliding of robot fingers under combined torsion and shear loading. In *IEEE International Conference on Robotics and Automation*, volume 1, pages 103–105, 1988.

[8] T. Huynh, C. Lassez, and J-L. Lassez. Practical issues on the projection of polyhedral sets. *Ann. Math. Artif. Intell.*, 6(4):295–315, 1992.

[9] J. R. Kerr and B. Roth. Analysis of multi-fingered hands. *The International Journal of Robotics Research*, 4(4), Winter 1986.

[10] Y.H. Liu and M. Wang. Qualitative test and force optimization of 3d frictional force-closure grasps using linear programming. In *"Proceedings of IEEE International Conference on Robotics and Automation", year = 1998, pages = 3335-3340,.*

[11] P. Lotstedt. Coulomb friction in two-dimensional rigid body systems. *Zeitschrift fur Angewandte Mathematik und Mechanik*, 61:605–615, 1981.

[12] M. T. Mason. Two graphical methods for planar contact problems. In *IEEE/RSJ International Conference on Intelligent Robots and Systems, Intelligence for Mechanical Systems*, volume 2, pages 443–448, November 1991.

[13] M. T. Mason and J. K. Salisbury. *Jr. Robots Hands and the Mechanics of Manipulation.* MIT Press, Cambridge, MA, 1985.

[14] M. T. Mason and Y. Wang. On the inconsistency of rigid-body frictional planar mechanics. In *IEEE Int. Conf. on Robotics and Aut.*, pages 524–528, 1988.

[15] R. Mason, J. W. Burdick, and E. Rimon. Stable poses of three-dimensional objects. In *IEEE Int. Conf. on Robotics and Automation*, Albuquerque NM, May 1997.

[16] R.B. McGhee and A.A. Frank. On the stability properties of quadruped creeping gaits. *Mathematical Biosciences*, 3(3–4):331–351, 1968.

[17] Y. Or and E. Rimon. Robust multiple contact postures in a two-dimensional gravitational field. In *IEEE Int. Conf. on Robotics and Automation*, pages 4783–4788, 2004.

[18] Y. Or and E. Rimon. Computation and graphic characterization of robust multiple-contact postures in gravitational environments. In *IEEE Int. Conf. on Robotics and Automation*, pages 248–253, 2005.

[19] J. S. Pang and J. C. Trinkle. Stability characterizations of fixtured rigid bodies with coulomb friction. In *IEEE Int. Conference on Robotics and Automation*, pages 361–368, 2000.

[20] J. Ponce, D. Stam, and B. Faverjon. On computing force-closure grasps of curved two-dimensional objects. *The International Journal of Robotics Research*, 12(3):263–273, June 1993.

[21] J. Ponce, S. Sullivan, A. Sudsang, J.-D. Boissonnat, and J.-P. Merlet. On computing four-finger equilibrium and force-closure grasps of polyhedral objects. *The Int. Journal of Robotics Research*, 16(1):11–35, February 1997.

[22] V. T. Rajan, R. Burridge, and J. T. Schwartz. Dynamics of rigid body in frictional contact with rigid walls. In *IEEE Int. Conf. on Robotics and Automation*, pages 671–677, 1987.

[23] G. Salmon. *Lessons Introductory to the Modern Higher Algebra*. Chelsea Publishing Co., New York, 1964.

[24] T. Sugihara and Y. Nakamura. Whole-body cooperative cog control through zmp manipulation for humanoid robots. In *2nd Int. Symp. on Adaptive Motion of Animals and Machines(AMAM2003)*, 2003.

[25] M. Vukobratovic, A.A. Frank, and D. Juricic. On the stability of biped locomotion. In *IEEE Trans Biomed Eng*, volume 17, pages 25–36, 1970.

Appendix - proof of Proposition 3.4

First, recall that criticality conditions also hold under change of coordinates. Second, notice that type-1, type-2 and type-3 curves lie in submainfolds of Q, whose dimensions are 4,3 and 2 respectively. For each of the possible types, we now choose a reduced set of new coordinates, and express the restriction $\bar{\Phi}$ of Φ to the corresponding sumbmanifold of Q with the new coordinates. Then we explicitly compute the Jacobian $D\bar{\Phi}$, and formulate the conditions for its rank deficiency.

Type-0 critical points: Type-0 curves correspond to contact forces $\vec{f_i}$ that lie in the interior of $\mathcal{C}_i$. In such case, we parametrize the horizontal components of the contact forces $\tilde{f_i}$ by the pair $(\boldsymbol{r}, \sigma) \in I\!R^2 \times I\!R$ as shown in lemma 3.1. Since Eq. (4b) defines a simple relation between the vertical components f_i^z, we now choose the coordinates $(\boldsymbol{r}, \sigma, f_1^z, f_2^z))$ to parametrize the contact forces. Using this change of coordinates, and substituting into Eq. (4c), the map Φ is defined in the new coordinates as follows:

$$\tilde{\boldsymbol{x}} = \Phi(\boldsymbol{r}, \sigma, f_1^z, f_2^z) = J\left[\sigma \cdot \sum_{i=1}^{3}[\bar{H}_i \lambda_i(\boldsymbol{r})(\boldsymbol{r} - \tilde{x_i})] + \bar{h}_1 f_1^z + \bar{h}_2 f_2^z + \bar{h}_3(1 - f_1^z - f_2^z)\right],$$

where $\lambda_i(\boldsymbol{r}) = (\boldsymbol{r} - \tilde{x}_{i+1}) \cdot J(\tilde{x}_{i+2} - \tilde{x}_{i+1})$, and the index i is taken modulo 3. The Jacobian matrix is a matrix of order 2×5, and its two last columns are $\frac{\partial \Phi}{\partial f_1^z} = \bar{h}_1 - \bar{h}_3$ and $\frac{\partial \Phi}{\partial f_2^z} = \bar{h}_2 - \bar{h}_3$. Since the full rank is 2, a necessary condition for rank deficiency is that the two last columns are linearly dependent. Recalling the definition of $\bar{h}_i$, one can see that this is true only if there exists a vertical plane (i.e. containing the vertical direction $\boldsymbol{e}$) that contains the three contact points in $I\!R^3$. In such a non-generic case, all contact forces must lie within this plane, reducing to the planar problem solved in [18].

Type-1 critical points: Type-1 curves correspond to contact forces $\vec{f_i}$ such that only one contact force lies on the boundary of its friction cone. Without loss of generality, assume that the contact forces $\vec{f_1}$ and $\vec{f_2}$ lie in the interior of their friction cones, while $\vec{f_3}$ lies on the boundary of $\mathcal{C}_3$. Using (10), this implies that $\zeta_3 = \tilde{b}_3^T(\boldsymbol{r} - \tilde{x}_3) \pm \sqrt{(\boldsymbol{r} - \tilde{x}_3)^T \tilde{B}_3 (\boldsymbol{r} - \tilde{x}_3)}$. The horizontal components $\tilde{f_i}$ can be parametrized by $(\boldsymbol{r}, \sigma)$ as above. We now parametrize the forces using the coordinates $(\boldsymbol{r}, f_1^z, f_2^z)$, and eliminating σ. The vertical component of $\vec{f_3}$ is $f_3^z = \sigma(\boldsymbol{r}, f_1^z, f_2^z)\lambda_3(\boldsymbol{r})\zeta_3(\boldsymbol{r})$. Eq. (4b) implies that $\sigma(\boldsymbol{r}, f_1^z, f_2^z) = (1 - f_1^z - f_2^z)/(\lambda_3(\boldsymbol{r})\zeta_3(\boldsymbol{r}))$. Using this change of coordinates, and substituting into Eq. (4c), the restricted map $\bar{\Phi}$ is defined in the new coordinates as follows:

$$\tilde{\boldsymbol{x}} = \bar{\Phi}(\boldsymbol{r}, f_1^z, f_2^z) = \left[\sigma(\boldsymbol{r}, f_1^z, f_2^z) \cdot \sum_{i=1}^{3}[\bar{H}_i \lambda_i(\boldsymbol{r})(\boldsymbol{r} - \tilde{x_i})] + \bar{h}_1 f_1^z + \bar{h}_2 f_2^z + \bar{h}_3(1 - f_1^z - f_2^z)\right],$$

where $\lambda_i(\boldsymbol{r}) = (\boldsymbol{r} - \tilde{x}_{i+1}) \cdot J(\tilde{x}_{i+2} - \tilde{x}_{i+1})$, and $\sigma(\boldsymbol{r}, f_1^z, f_2^z)$ is defined above. The first two columns of the 2×4 Jacobian matrix are the matrix

$$\frac{\partial \bar{\Phi}}{\partial \boldsymbol{r}} = (1 - f_1^z - f_2^z) \cdot \frac{\partial}{\partial \boldsymbol{r}}\left(\frac{1}{\lambda_3(\boldsymbol{r})\zeta_3(\boldsymbol{r})} \sum_{j=1}^{3}[\bar{H}_j \lambda_j(\boldsymbol{r})(\boldsymbol{r} - \tilde{x_j})]\right).$$

The last two columns of the Jacobian matrix are

$$\frac{\partial \bar{\Phi}}{\partial f_i^z} = \bar{h}_i - \bar{h}_3 - \frac{1}{\lambda_3(\boldsymbol{r})\zeta_3(\boldsymbol{r})} \sum_{j=1}^{3}[\bar{H}_j \lambda_j(\boldsymbol{r})(\boldsymbol{r} - \tilde{x_j})], \text{ for } i = 1, 2.$$

Since the factor $(1 - f_1^z - f_2^z)$ multiplies two columns of the Jacobian matrix, it does not affect its rank as long as it is nonzero. In such case, the condition for rank deficiency of the 2×4 Jacobian matrix gives three scalar equations in $\boldsymbol{r} \in I\!R^2$, which are generically independent, and hence have no solution. The case $(1 - f_1^z - f_2^z) = 0$ yields $f_3^z = 0$. Since we assumed upward pointing contacts, $\vec{f_3}$ must vanish. In this case, $\boldsymbol{r}$ must lie on the line passing through $\tilde{x}_1$ and $\tilde{x}_2$, and the contact forces $\vec{f_1}$ and $\vec{f_2}$ must lie within the vertical plane containing x_1 and x_2, reducing to the planar problem solved in [18].

Type-2 critical points: Type-2 curves correspond to contact forces $\vec{f_i}$ such that two contact force lie on the boundary of their friction cones. Without loss of generality, assume that the contact force $\vec{f_1}$ lies in the interior of its friction cone, while $\vec{f_2} \in \partial\mathcal{C}_2$ and $\vec{f_3} \in \partial\mathcal{C}_3$. Using (10), this implies that $\zeta_i = \tilde{b}_i^T(\boldsymbol{r} - \tilde{x}_i) \pm \sqrt{(\boldsymbol{r} - \tilde{x}_i)^T \tilde{B}_i (\boldsymbol{r} - \tilde{x}_i)}$ for $i = 2, 3$. The horizontal components $\tilde{f}_i$ can be parametrized by $(\boldsymbol{r}, \sigma)$ as above. We now parametrize the forces using the coordinates $(\boldsymbol{r}, f_1^z)$, and eliminating σ. The vertical components are $f_i^z = \sigma(\boldsymbol{r}, f_1^z)\lambda_i(\boldsymbol{r})\zeta_i(\boldsymbol{r})$ for $i = 2, 3$. Eq. (4b) implies that $\sigma(\boldsymbol{r}, f_1^z) = (1 - f_1^z)/(\lambda_2(\boldsymbol{r})\zeta_2(\boldsymbol{r}) + \lambda_3(\boldsymbol{r})\zeta_3(\boldsymbol{r}))$. Using this change of coordinates, and substituting into Eq. (4c), the restricted map $\bar{\Phi}$ is defined in the new coordinates as $\tilde{\boldsymbol{x}} = \bar{\Phi}(\boldsymbol{r}, f_1^z) = (1 - f_1^z)\boldsymbol{u}(\boldsymbol{r}) + \bar{h}_1 f_1^z$, where $\boldsymbol{u}(\boldsymbol{r})$ is defined in (14). The 2×3 Jacobian matrix is

$$D\bar{\Phi} = \left[(1 - f_1^z)\tfrac{\partial}{\partial \boldsymbol{r}}\boldsymbol{u}(\boldsymbol{r}) \quad \bar{h}_1 - \boldsymbol{u}(\boldsymbol{r})\right].$$

Differentiating $\bar{\Phi}$ using the chain rule gives

$$\tfrac{d}{d\boldsymbol{r}}\boldsymbol{u}(\boldsymbol{r}) = \tfrac{\partial \boldsymbol{u}}{\partial \boldsymbol{r}} + \sum_{i=1}^{3} \tfrac{\partial \boldsymbol{u}}{\partial \lambda_i}\tfrac{\partial \lambda_i}{\partial \boldsymbol{r}} + \tfrac{\partial \boldsymbol{u}}{\partial \zeta_i}\tfrac{\partial \zeta_i}{\partial \boldsymbol{r}} = \tfrac{1 - f_1^z}{(\lambda_2\zeta_2 + \lambda_3\zeta_3)^2} M_2(\boldsymbol{r}),$$

where $M_2(\boldsymbol{r})$ is defined in Eq. (13). Since the factor $(1 - f_1^z)$ multiplies two columns of the Jacobian matrix, it does not affect its rank as long as it is nonzero. In case $f_1^z = 1$, the Jacobian $D\bar{\Phi}$ is not full rank. Using Eq. (4c) gives $f_2^z + f_3^z = 0$. The assumption of upward pointing contacts implies that $\vec{f_2}, \vec{f_2} \geq 0$, and hence $\vec{f_2}$ and $\vec{f_3}$ must vanish. In this case, $\boldsymbol{r} = \tilde{\boldsymbol{x}} = \tilde{x}_1$, i.e. the center-of-mass lies on the vertical line passing through the contact x_1. This case is possible only if the friction cone $\mathcal{C}_1$ contains the vertical direction $\boldsymbol{e}$.

In case $f_1^z \neq 1$, the condition for rank deficiency of the 2×3 Jacobian matrix is that the determinants of the two first columns and of the two last columns vanish simultaneously. This gives two scalar equations in $\boldsymbol{r} \in I\!R^2$ which are generically independent, and the solution is a finite set of isolated critical points $\boldsymbol{r}^*$. Therefore, the critical curves are straight line, on which $\boldsymbol{r}$ is fixed, ζ_2, ζ_3 are determined by $\boldsymbol{r}$ as in (10), and ζ_1 is free. Notice that there are three possible permutations of the contacts' indices, resulting in three possible cases of type-2 critical curves.

In the special case where all the contacts are located at equal heights, locating the reference frame at that height gives $\bar{H}_i = 0_{2\times 2}$ for $i = 1, 2, 3$. One can show that in such case, the matrix $M_2(\boldsymbol{r})$ is always singular. Therefore, $D\bar{\Phi}$ is of rank 1 on a two-dimensional manifold in $(\boldsymbol{r}, f_1^z)$-space. Since $\bar{\Phi}$ is linear in f_1^z, for any constant $\boldsymbol{r}$ its extreme values occur where f_z^1 reaches its extreme values and $\vec{f_1}$ lies on the boundary of $\mathcal{C}_1$. Hence, the corresponding boundary curves can be computed also as Φ-image of type-3 critical curves.

Type-3 critical points: Type-3 curves correspond to contact forces $\vec{f_i}$ such that all contact force lie on the boundary of their friction cones. Using (10), this implies that

$\zeta_i = \tilde{b}_i^T(\boldsymbol{r} - \tilde{x}_i) \pm \sqrt{(\boldsymbol{r} - \tilde{x}_i)^T \tilde{B}_i (\boldsymbol{r} - \tilde{x}_i)}$ for $i = 1, 2, 3$. Substituting into Eq. (7) and Eq. (9) gives the following restricted map $\bar{\Phi}(\boldsymbol{r})$:

$$\begin{aligned}
&\bar{\Phi}(\boldsymbol{r}) = \sigma(\boldsymbol{r}, \boldsymbol{\zeta}) \textstyle\sum_{i=1}^3 \lambda_i(\boldsymbol{r})[\bar{H}_i(\boldsymbol{r} - \tilde{x}_i) + \bar{h}_i \zeta_i(\boldsymbol{r})], \text{ where} \\
&\sigma(\boldsymbol{r}, \boldsymbol{\zeta}) = 1/\textstyle\sum_{j=1}^3 \lambda_j(\boldsymbol{r}) \zeta_j(\boldsymbol{r}) \\
&\lambda_i(\boldsymbol{r}) = (\boldsymbol{r} - \tilde{x}_{i+1}) \cdot J(\tilde{x}_{i+2} - \tilde{x}_{i+1}), \text{ and } \zeta_i(\boldsymbol{r}) \text{ are defined above.}
\end{aligned} \tag{22}$$

Critical curves are points $\boldsymbol{r}$ at which the 2×2 Jacobian matrix $D\bar{\Phi}$ loses full rank. Using the chain rule, this matrix is computed by composition of the following:

$$\begin{aligned}
D\bar{\Phi} &= \tfrac{\partial \bar{\Phi}}{\partial \boldsymbol{r}} + \tfrac{\partial \bar{\Phi}}{\partial \sigma} \tfrac{\partial \sigma}{\partial \boldsymbol{r}} + \textstyle\sum_{j=1}^3 \left(\tfrac{\partial \bar{\Phi}}{\partial \sigma} \tfrac{\partial \sigma}{\partial \zeta_j} + \tfrac{\partial \bar{\Phi}}{\partial \zeta_j} \right) \tfrac{\partial \zeta_j}{\partial \boldsymbol{r}} \\
\tfrac{\partial \bar{\Phi}}{\partial \boldsymbol{r}} &= \sigma(\boldsymbol{r}, \boldsymbol{\zeta}) J \textstyle\sum_{i=1}^3 \left[(H_i(\boldsymbol{r} - \tilde{x}_i) + h_i \zeta_i(\boldsymbol{r}))(\tilde{x}_{i+2} - \tilde{x}_{i+1})^T J^T + \lambda_i(\boldsymbol{r}) H_i \right] \\
\tfrac{\partial \bar{\Phi}}{\partial \sigma} &= J \textstyle\sum_{i=1}^3 \lambda_i(\boldsymbol{r})[H_i(\boldsymbol{r} - \tilde{x}_i) + h_i \zeta_i(\boldsymbol{r})] \\
\tfrac{\partial \sigma}{\partial \boldsymbol{r}} &= -\sigma(\boldsymbol{r}, \boldsymbol{\zeta})^2 \textstyle\sum_{i=1}^3 \zeta_j (\tilde{x}_{i+2} - \tilde{x}_{i+1})^T J^T \\
\tfrac{\partial \sigma}{\partial \zeta_j} &= -\sigma(\boldsymbol{r}, \boldsymbol{\zeta})^2 \lambda_j(\boldsymbol{r}) \\
\tfrac{\partial \bar{\Phi}}{\partial \zeta_j} &= \sigma(\boldsymbol{r}, \boldsymbol{\zeta}) J h_i \lambda_j(\boldsymbol{r}) \\
\tfrac{\partial \zeta_j}{\partial \boldsymbol{r}} &= \tilde{b}_j^T \pm \tfrac{1}{\sqrt{(\boldsymbol{r} - \tilde{x}_j)^T \tilde{B}_j (\boldsymbol{r} - \tilde{x}_j)}} (\boldsymbol{r} - \tilde{x}_j)^T \tilde{B}_j.
\end{aligned}$$

The rank deficiency condition is $\det(D\bar{\Phi}) = 0$. Substituting the partial derivatives listed above into $D\bar{\Phi}$, rearranging and multiplying by $[\sigma(\boldsymbol{r}, \boldsymbol{\zeta})]^{-2}$ gives the matrix $M_3(\boldsymbol{r})$ defined in the proposition. □